Proceedings of the 2003 IEEE/ASME
International Conference on
Advanced Intelligent Mechatronics (AIM 2003)

Novel Design of a 6-DOF Planar Maglev Positioning System

Mei-Yung Chen
Dept. of Electrical Engineering, National Taiwan University, Taipei, Taiwan, Republic of China.
email cmy@cc.ee.ntu.edu.tw

Tzuo-Bo Lin
Dept. of Electrical Engineering, National Taiwan University, Taipei, Taiwan, Republic of China.
email lichen@ccms.ntu.edu.tw

Ming-Chiuan Shiu
Dept. of Electrical Engineering, Hsiuping Institude of Technology, Taichung, Taiwan, Republic of China.
email smc@mail.hit.edu.tw

Li-Chen Fu
Dept. of Electrical Engineering,, National Taiwan University, Taipei, Taiwan, Republic of China.
email lichen@ccms.ntu.edu.tw

Abstract

A novel 6-DOF magnetic levitation (Maglev) system is proposed in this paper. In this system, both new structure and adaptive control algorithm are developed. Three objectives we attempt to achieve simultaneously include large moving range, accurate positioning, and fast response. Structurally, totally there are six permanent magnets (PMs) attached on the carrier, while six coils mounted on a fixed part. By analyzing the magnetic force characteristics between permanent magnets and coils, the general model of this system with full DOFs is therefore derived and analyzed. Then, due to the naturally unstable behavior and uncertainties of the Maglev systems, an adaptive controller is proposed to guarantee the stabilities of all DOFs both in regulation and tracking. From the experimental results, satisfactory good performances including stiffness and precision have been demonstrated.

Keywords

Maglev, Precision positioning, Adaptive controller.

INTRODUCTION

With the progress of the industrial technologies, high-precision positioning system plays an important role in various high-tech fields. To meet these challenging needs, more stringent manufacturing processes and advanced fabrication equipments, therefore, should be developed. In traditional mechanical actuators, mostly the piezoelectric actuators [1][2] only handle the small moving range, the ball-screws [3][4] cause disturbances and backlash due to roughness of the bearing elements, and the linear motors have ripple effect in a motion stroke. It is generally believed that magnetic levitation system not only achieves advantages that the previous two actuators possess but even overcome their shortcomings as well.

Based on the design theories and experience for developing single-axis and dual-axis Maglev guiding systems [5][6], a new planar Maglev system is proposed in this paper. There are six PMs attached on the moving part so-called carrier, while six coils mounted on a fixed part. Three of these six coils are arranged in the bottom and mainly generate levitating forces as well as torques around X- and Y- axis. And

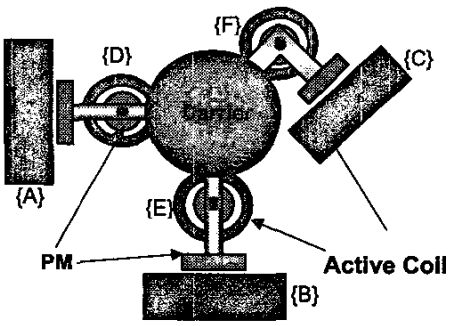

Figure 1. Conceptual configuration

the three side-coils with rectangle shaped mainly produce lateral forces and torque around Z-axis as well. The conceptual configuration and photograph of this system are shown in Fig. 1 and Fig. 2, respectively.

In this paper, first, the dynamic model with full DOFs is analyzed. Then, an adaptive controller which deals with unknown parameters is proposed to control the carrier at the desired target point. To demonstrate the performance of the entire system, experimental results are provided for verification. The organization of this paper is as follows. The detailed description of the complete dynamics will be given in Section 2. And Section 3 concentrates on the system controller design. Section 4 is about the experimental results as well as some discussions. Finally, conclusions are given in Section 5.

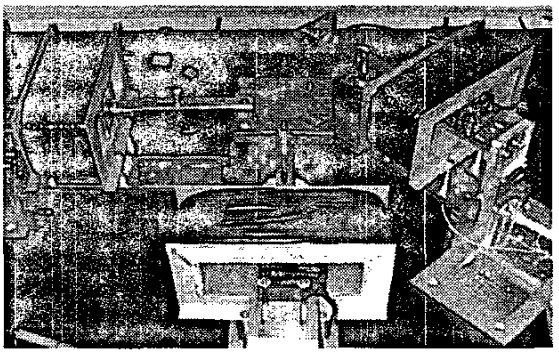

Figure 2. Photograph of the planar Maglev system

MAGLEV SYSTEM DESCRIPTION AND MODELING

About this system, it can be regarded composed of six sub-systems. The upper three sub-systems and the lower three have different pairs of coil and PM. They are rectangular and cylindrical respectively. To model this system, the interactions between coil and PM become a very important issue. So in this section it begins with two approaches, which are introduced to model these interactions. And then this modeling result will be integrated to develop the general model of this system.

Analysis of magnetic force characteristics

First, we try to model the interactions from the analytic approach by utilizing several useful fundamental theorems in electromagnetics. The force $\vec{F}$ and torque $\vec{T}$ exerted on a PM, which is exposed in an external magnetic field $\vec{H}$ can be obtained from the *Lorentz force*:

$$\vec{F} = (\vec{m} \cdot \nabla)\mu_0 \vec{H} \quad , \tag{1}$$

$$\vec{T} = \vec{m} \times (\mu_0 \vec{H}) \quad , \tag{2}$$

where $\vec{m}$ denotes the dipole moment of the PM and μ_0 is the permeability of free space equal to $4\pi \times 10^{-7}$(H/m). In this system it is assumed that each PM can be viewed as a single magnetic dipole moment with the direction perpendicular to its surface. So how to derive the magnetic field $\vec{H}$ becomes an important task in this research.

From *Biot-Savart Law* [7], the magnetic field $\vec{H}$ can be expressed as:

$$\vec{H} = \frac{1}{4\pi} \int_{v'} \frac{\vec{J}(\vec{r}') \times \vec{i}_{r'r} dv'}{|r' - r|^2} \quad , \tag{3}$$

where $\vec{J}$ is the current density, $\vec{r}'$ is the source coordinate, $\vec{r}$ represents the observer coordinate, $\vec{i}_{r'r}$ is a unit vector $\vec{i}_{r'r}$ directed from $\vec{r}'$ to $\vec{r}$. And dv' is a tiny cube of the current source.

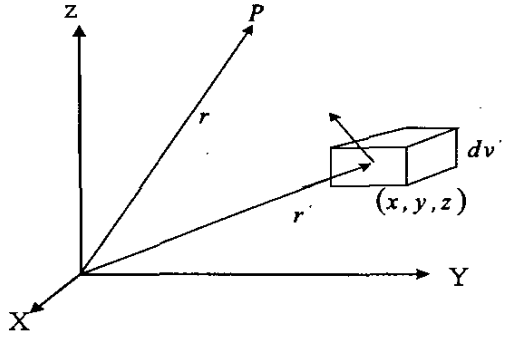

Figure 3. Spatial relations between current source dv' with coordinate $\vec{r}'$ and arbitrary observer P with coordinate $\vec{r}$.

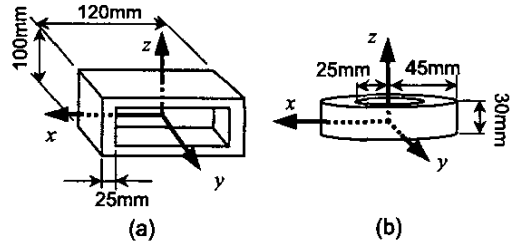

Figure 4. Specifications of (a) rectangular and (b) cylindrical coil used in this system.

The whole spatial relations are shown in Fig. 3. Many researches have been successfully done for estimating the magnetic field which is produced from coil by utilizing Eq.(3) and the skill of superposition integral. Mostly, those researches focus on cylindrical solenoid. However, due to the requirement of large traveling range, the shape of the three side-coils in this system is thus chosen as rectangle. In general, it is very difficult to model the magnetic field generated by rectangular coils.

However, this analytic approach still provides some useful information. The first, from Eq.(3), the magnetic field $\vec{H}$ is proportional to the current flowing into the coil. Second, $\vec{H}$ varies with the change of PM's position relative to the coil. Recalling Eq.(1), it is not hard to find that the magnetic force $\vec{F}$ is also proportional to the coil's current and a function of PM's position. As a result, these behaviors can be written in mathematic form as shown below:

$$\vec{F} = \vec{g}(x, y, z)u \quad , \tag{4}$$

where $\vec{g}$ is a function of PM's position and u denotes the current flowing into coil. Based on Eq.(4), the other approach will be introduced in the following subsection.

Measurement of magnetic force

A simpler and even more accurate approach, direct measurement, is adopted here. In this research, a force detector is used to measure the force exerted on the PM in the coil's magnetic field. The windings of two kinds of coils used in this system are made of copper with diameter equal to 0.65 mm. And the other details are shown in Fig. 4, where both two origins of coordinate are located on the centers of these two kinds of coils respectively.

First we consider the rectangular coil. Within our desired traveling range $\pm$4mm, the magnetic force distributed on x- and z-axis is much smaller than it distributed on y-axis. So we only take care the force exerted along its y-axis and treat the force distributed in other axes as disturbance. Therefore, from Eq. (4), this magnetic force $F_{rec,y}$ along its y-axis would be:

$$F_{rec,y} = g_{rec,y}(x, y, z)u_{rec} \quad , \tag{5}$$

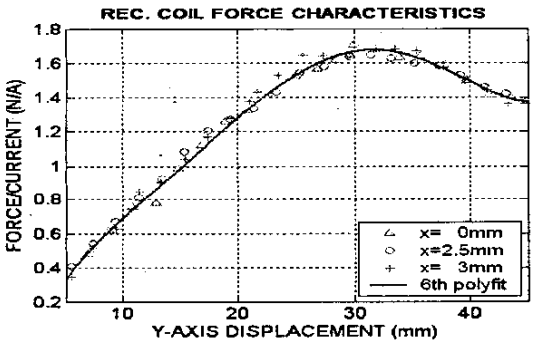

Figure 5. Magnetic force along its y-axis in rectangular coil.

where u_{rec} is the current flowing into rectangular coil. Then the magnetic force along its y-axis $F_{rec,y}$ in rectangular coil is measured.

And this measured result is shown in Fig. 5, where 'Δ' represents data on x=0mm, 'o' represents data on x=2.5mm, '+' represents data on x=5mm, and the solid line is the 6th polynomial fit that will be mentioned later. From this result, it is not hard to discover that $F_{rec,y}$ with different displacements along x-axis are very close. In this result, the largest mismatch in this three data-line is even within 8%.

Additionally, in most Maglev system including ours, the carrier is usually levitated at a specific height. This implies that the PM's displacement in z-axis is very small and thus its influence on the force is limited. So for the reason of convenience and simplification, the force characteristics within the desired traveling range are regarded as identity, i.e. $g_{rec,y}(x, y, z)$ in Eq.(5) can be represented by $g_{rec,y}(y)$. Then a polynomial fit is used to approximate those measured data. This fitting result is shown in Eq.(6) and plotted in Fig. 5.

$$F_{rec,y} = (a_6 y^6 + a_5 y^5 + a_4 y^4 + a_3 y^3 + a_2 y^2 + a_1 y + a_0) u_{rec}, \quad (6)$$

where a_6=-1.954 x 10^9, a_5=4.39 x 10^8, a_4=-3.385 x 10^7, a_3=1.16x10^5, a_2=-19338, a_1=214.8, and a_0=-0.385.

Similarly, the same method can be applied to cylindrical solenoid. And the result of its polynomial fit is shown below:

$$F_{cyl,z} = (b_4 z^4 + b_3 z^3 + b_2 z^2 + b_1 z + b_0) u_{cyl}, \quad (7)$$

where b_4=-4.87x10^6, b_3=-6.522x10^5, b_2=-33486, b_1= -736.02, and b_0= -4.166.

Development of the overall model

To develop the overall model of this system, the global coordinate is first defined. Its origin is just located on where the center of the carrier is operated nominally. This concept combining with the force relations are shown in Fig. 6.

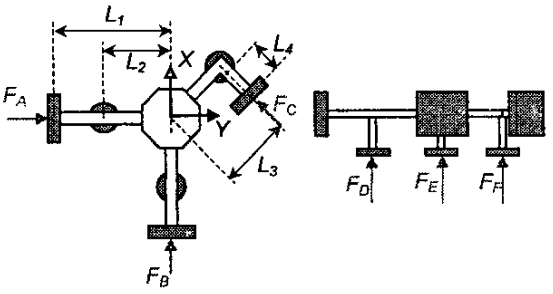

Figure 6. Carrier structure and force relation. (a) Top view of the carrier. (b) Front view of the carrier.

Then, some assumptions are made. First, it is assumed that the mutual effects between each subsystem are very small and can be ignored. The second, in our operations, the performance of carrier's translation is mainly concerned and its rotation is just regulated.

That means the angular displacement of the carrier around each axis is very small. Due to these small angular displacements, it is assumed that the attitude around Z-axis will not be coupled with that around the other two axes. Due to the system's structure, the total forces and torques equations can be expressed as:

$$\begin{aligned}
\sum F_X &= F_A - \sqrt{2}/2\, F_C, \\
\sum F_Y &= F_B + \sqrt{2}/2\, F_C, \\
\sum F_Z &= F_D + F_E + F_F - Mg, \\
\sum T_X &= -F_E L_2 + \sqrt{2}/2\, F_F L_3, \\
\sum T_Y &= F_D L_2 - \sqrt{2}/2\, F_F L_3, \\
\sum T_Z &= F_C L_3,
\end{aligned} \quad (8)$$

where M=0.413kg, L_1=0.16m, L_2=0.1m, L_3=0.12m, and L_4=0.06m.

Initially, in upper sub-systems, each PM is located on y=$p_{rec,0}$ in the local coordinate of its facing rectangular coil while each PM in lower subsystems is located on z=$p_{cyl,0}$ in the local coordinate of its facing cylindrical coil. In this system, $p_{rec,0}$ is equal to 30mm, and $p_{cyl,0}$ is -20mm.

Once the carrier undergoes a translation $[X, Y, Z]^T$ and a rotation $[\varphi, \phi, \theta]^T$, each relative position between PM and coil will be changed. Each relative displacement in its coordinate is then written as:

$$y|_A = p_{rec,0} + X + L_1 (1 - \cos\theta),$$

$$
\begin{aligned}
y|_B &= p_{rec,0} + Y + L_1(1-\cos\theta) \\
y|_C &= p_{rec,0} + \sqrt{2}/2(-X+Y) + (L_3^2 + L_4^2)^{1/2}\sin\theta \\
z|_D &= p_{cyl,0} + Z + L_2\sin\phi \\
z|_E &= p_{cyl,0} + Z - L_2\sin\varphi \\
z|_F &= p_{cyl,0} + Z + \sqrt{2}/2\, L_3(\sin\varphi - \sin\phi)
\end{aligned}, \quad (9)
$$

Then, by substituting Eq.(9) into Eq.(6) and Eq.(7), the forces with the subscript of A~F in Eq. (8) can be obtained. From *Newton Euler's Law*, the dynamics of this system can be written as:

$$
\begin{aligned}
\sum F_X &= M\ddot{X} \\
\sum F_Y &= M\ddot{Y} \\
\sum F_Z &= M\ddot{Z} \\
\sum T_X &= I_{XX}\ddot{\varphi} + (I_{ZZ} - I_{YY})\dot{\phi}\dot{\theta} \cong I_{XX}\ddot{\varphi} \\
\sum T_Y &= I_{YY}\ddot{\phi} + (I_{XX} - I_{ZZ})\dot{\varphi}\dot{\theta} \cong I_{YY}\ddot{\phi} \\
\sum T_Z &= I_{ZZ}\ddot{\theta} + (I_{YY} - I_{XX})\dot{\varphi}\dot{\phi} \cong I_{ZZ}\ddot{\theta}
\end{aligned}, \quad (10)
$$

where I_{XX} =0.000101kg-m^2, I_{YY} = 0.000101 kg-m^2, and I_{ZZ} = 0.00032 kg-m^2. So far, the overall model can be derived by combining Eq.(6~10).

CONTROLLER DESIGN

In order to simplify notations in the following derivations, the system's model can be written into the state-space form as:

$$
\bar{M}\ddot{E} = B(E)U + W_1, \quad (11)
$$

where $\bar{M} = diag[M, M, M, I_{xx}, I_{yy}, I_{zz}]$ is the mass matrix, $E = [X, Y, Z, \varphi, \phi, \theta]^T$ is error state variable , $B(.)$ is a square matrix and invertible within our operating range, $U = [u_1, u_2, u_3, u_4, u_5, u_6]^T$ is control input, and W_1 denotes the uncertainty.

Before the design of adaptive controller, we first linearize Eq.(11) at operation point E_0=[0, 0, 0, 0, 0, 0]^T with bias current U_0=[0, 0, 0, 1.326, 1.326, 1.68]^T. Then the linearized equation is shown below:

$$
\bar{M}\ddot{E} = B_0U + W_2, \quad (12)
$$

where B_0 is a constant matrix. Note that W_1 combining with the high order terms left out from linearization are aggregated into the term W_2.

Controller Design

Rewrite the Eq.(12)

$$
B_0^{-1}\bar{M}\ddot{E} = U + B_0^{-1}W_1 \Rightarrow D_B\ddot{E} = U + v. \quad (13)
$$

Thus, a compact form of the overall system model is derived. Then, assume a sliding surface S, with the following form:

$$
S = G_D\dot{E} + G_PE, \quad (14)
$$

where G_D, G_P>0. In this application, we try to regulate state error E to zero, which simultaneously regulates the derivative of E to zero as well. Due to this reason, if the sliding surface tends to zero within finite time can be proved, then E and $\dot{E}$ are also forced to zero exponentially. To relate the sliding surface to the dynamics of motion, we find out the time derivative of the sliding surface is:

$$
\dot{S} = G_D\ddot{E} + G_P\dot{E}. \quad (15)
$$

As described in the previous section, an adaptive controller is applied in this research, which is capable of estimating parameters of the system on-line while controlling the system simultaneously. After we have the estimates of system parameters, Eq.(15) with these estimates in the control command can be used. So, we substitute the estimates acquired from the on-line estimator and derive the following:

$$
U = \hat{D}_B G_D^{-1}(-KG_D\dot{E} - KG_PE - G_PE) - \hat{v} - sat(S), \quad (16)
$$

where K>0, $\hat{D}_B$ and $\hat{v}$ are the estimated values of D_B and v, respectively, and $sat(.)$ is the saturation function defined as:

$$
sat(S) = \begin{cases} 1 & S > \varepsilon \\ \dfrac{S}{|\varepsilon|} & if \quad \varepsilon \geq S \geq -\varepsilon \\ -1 & S < -\varepsilon \end{cases}. \quad (17)
$$

Thus, substituting Eq.(16) into Eq.(13), we can obtain

$$
\begin{aligned}
D_B[G_D^{-1}\dot{S} + K(G_D^{-1}S)] &= \tilde{v} \\
&+ \tilde{D}_B(-KG_D^{-1}S - G_D^{-1}G_P\dot{E}) - sat(S),
\end{aligned} \quad (18)
$$

where the estimation errors are defined as $\tilde{D}_B = D_B - \hat{D}_B$ and $\tilde{v} = v - \hat{v}$. By applying appropriate gains K, G_D and G_P, we can accelerate the convergence and force them to zero in a shorter period of time.

Stability Analysis

In the previous section, we have derived the close-loop function in Eq.(18), which involves estimation errors. Now, with the help of estimator based on adaptive control theory, we then can derive the estimates, so that appropriate control commands are also derived.

We define a *Lyapunov function candidate* V [8], which is a positive definite function:

$$
\begin{aligned}
V = \frac{1}{2}\{&[D_B(G_D^{-1}S)]^T[D_B(G_D^{-1}S)] \\
&+ tr[(\tilde{D}_B)^T D_B\Gamma_1^{-1}(\tilde{D}_B)] + tr[(\tilde{v})^T D_B\Gamma_2^{-1}(\tilde{v})]\},
\end{aligned} \quad (19)
$$

where Γ_1^{-1} and Γ_2^{-1} are all positive diagonal matrixes. First, the time derivative of the *Lyapunov candidate function V* can be found out as:

$$\dot{V} = [D_B(G_D^{-1}S)]^T[D_B(G_D^{-1}\dot{S})] + tr[(\dot{\bar{D}}_B)^T D_B\Gamma_1^{-1}(\dot{\bar{D}}_B)] + tr[(\dot{\bar{v}})^T D_B\Gamma_2^{-1}(\dot{\bar{v}})], \quad (20)$$

along the solution trajectory of S in Eq.(14). Then, it can be rearranged by means of Eq.(20) into the following:

$$\begin{aligned}\dot{V} = &-[D_B(G_D^{-1}S)]^T[D_BK(G_D^{-1}S)] - [D_B(G_D^{-1}S)]^T[D_BG_D^{-1}sat(S)] \\ &+tr[(\dot{\bar{D}}_B)^T D_B\Gamma_2^{-1}(\dot{\bar{D}}_B) \\ &+(\dot{\bar{D}}_B)^T D_B(G_D^{-1}S)(-KG_D^{-1}S - G_D^{-1}G_P\dot{E})^T] \\ &+tr[(\dot{\bar{v}})^T D_B\Gamma_3^{-1}(\dot{\bar{v}}) + (\dot{\bar{v}})^T D_B(G_D^{-1}S)] \end{aligned} \quad (21)$$

Now, we derive adaptive laws as follows:

$$\begin{aligned}&\dot{\bar{D}}_B = -\dot{\bar{D}}_B = \Gamma_2(G_D^{-1}S)(-KG_D^{-1}S - G_D^{-1}G_P\dot{E})^T, \\ &\dot{\bar{v}} = -\dot{\bar{v}} = \Gamma_3(G_D^{-1}S)\end{aligned} \quad (22)$$

If these equations hold, Eq.(20) will become

$$\begin{aligned}\dot{V} &= -S^TG_D^{-1}D_B^TD_BKG_D^{-1}S - S^TG_D^{-1}D_B^TD_BG_D^{-1}sat(S) \le 0 \\ &= \begin{cases} -S^TG_D^{-1}D_B^TD_BKG_D^{-1}S - KS \le 0 & S > \varepsilon \\ -S^TG_D^{-1}D_B^TD_BKG_D^{-1}S - K\dfrac{S^2}{\varepsilon} \le 0 & S < \varepsilon \end{cases}\end{aligned}, \quad (23)$$

because G_D^{-1}, D_B and K are all positive diagonal matrices, thus they are commutable in deriving the inequality. And Eq.(23) also implies that the equilibrium $D_B = \hat{D}_B$ and $v = \hat{v}$ of the respective equations is uniformly bounded. Thus, by using *Barbalat's Lemma* [8] we establish that $S \in L_2$, $\dot{S} \in L_\infty$ and that: $|S(t)| \to 0$, $\|\dot{\bar{D}}_B\| \to 0$ and $\|\dot{\bar{v}}\| \to 0$ as $t \to \infty$.

Due to zero convergence of S, it can be readily verified that E coverage to zero asymptotically. In other words, state variables and time derivatives all converge to zero eventually, which is the goal of designing the controller for this system.

EXPERIMENTAL RESULTS

The experimental hardware, including the main body, sensor system, driver system and controller hardware, will be described here. A number of experimental results, including the regulation, step test, and rotational tracking will also be provided in this section to demonstrate performance of this system with the controller presented in section 3.

Experimental Hardware

For the reason of avoiding the EMI effects and the requirement of long traveling range, an optical sensor is therefore chosen in this experiment. Its sampling frequency is 10kHz whereas the active range up to 8mm and resolution of 10μm.

That means this sensor is fast enough and can cover all the traveling range in this application. The drivers are linear drivers designed to be servo drivers for DC motors. The current microcomputer is an IBM PC with Pentium-III 733 MHz microprocessor inside.

System performance

Figure 7 shows the regulation response with initial position on X= -1mm. From the trajectories of state, one can see that the error signals converge to their steady states within about 0.5s. The final precision is made up 10μm in translation, which is estimated to reach a limit of the sensor device. Meanwhile, the response in Z-axis is shown in Fig. 8. One might find there is still a slight perturbation on Z-axis as the instant movement of the carrier on X-axis. Due to the successful design of controller, this positioning error converges to zero very soon.

Figure 9 shows 1mm step input control test. The repeatable accuracy is about 10μm with transient time within 0.5s. This test shows that this system can achieve the three objectives involved in fast response, long traveling range, and precise positioning. Additionally, thought some assumptions about the angular displacement have been made in the process of modeling, the tracking capability of rotation is quit satisfactory as shown in Fig. 10.

From the experimental process, the adaptive controller, which can on-line perform system identification implicitly or explicitly while tuning the controller gains to guarantee the stability of the closed- loop system.

CONCLUSION

In this paper, we designed a precision Maglev system for large moving range. The dynamics of the Maglev system has been thoroughly analyzed and then a complete model also has been derived. The system is treated as a MIMO system, and an adaptive controller has been designed here and implemented using a microcomputer. By experimentation, excellent performance indices have been observed which ascertain that the three objectives were successfully achieved, large traveling range, precision positioning, and fast response are achieved.

ACKNOWLEDGMENTS

This research is sponsored by National Science Council, R.O.C., under the grant NSC- 90-2213-E -003–054.

REFERENCE

[1] Sitti, M. and Hashimoto, H., "Two-dimensional fine particle positioning using a piezoresistive cantilever as a micro/nano-manipulator", *1999 IEEE International Conference on Robotics and Automation*, Vol. 4, 1999. pp. 2729 –2735.

[2] Hector M. Gutierrez, Paul I. Ro. "Sliding-Mode Control of a Nonlinear-Input System: Application to a Magnetically Levitated Fast-Tool Servo", *IEEE Tran. on Industrial Electronics* ,Vol. 45, no. 6, 1998, pp. 921 –927.

[3] Li Xu and Bin Yao, "Adaptive robust precision motion control of linear motors with negligible electrical dynamics: theory and experiments", *IEEE/ASME Tran. on Mechatronics*, Vol. 6 Issue: 4 , 2001, pp. 444 –452.

[4] Pai-Yi Huang, Yung-Yew Chen and Min-Shin Chen "Position-dependent friction compensation for ball-screw tables", *Proceedings of the 1998 IEEE International Conference on Control Applications*, Vol. 2 , 1998, pp. 863 –867.

[5] Chen, M. Y., Wu, K. N. and Fu, L. C., "Design, Implementation and Self-tuning Adaptive Control of a Maglev Guiding System", *Mechatronic*, pp. 215-237, 2000.

[6] Chen, M. Y., Chin-Chung Wang. and Fu, L.C., "Adaptive Sliding Mode Controller Design of a Dual-Axis Maglev Positioning System", *American Control Conference*, 2001.

[7] J. G. David, *Introduction to Electrodynamics*. Prentice-Hall, Inc., Englewood Cliffs, New Jersey, 1981.

[8] Jean-Jacques E. Slotine, Weiping Li., *Applied nonlinear control*, Prentice Hall, 1990.

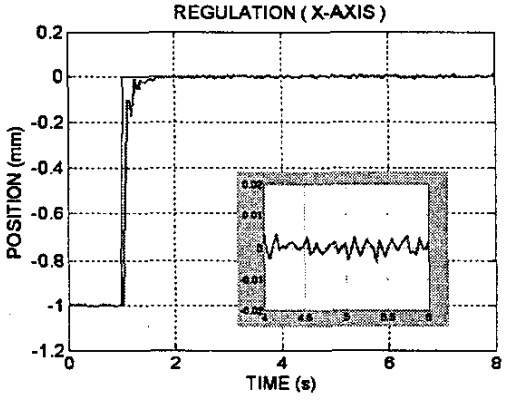

Figure 7. Regulation response on X-axis.

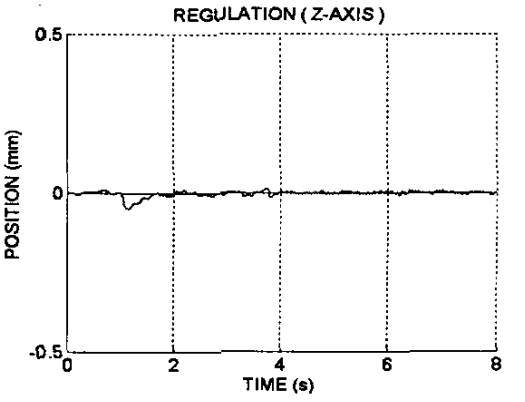

Figure 8. Regulation response on Z-axis.

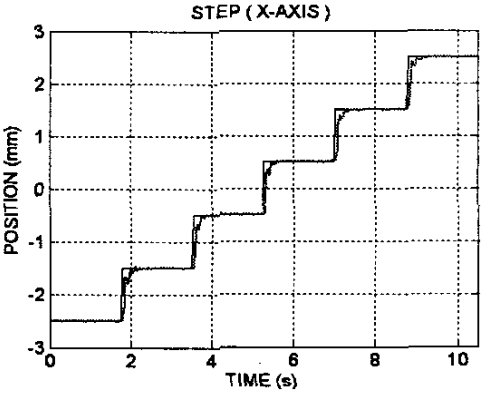

Figure 9. Step response on X-axis.

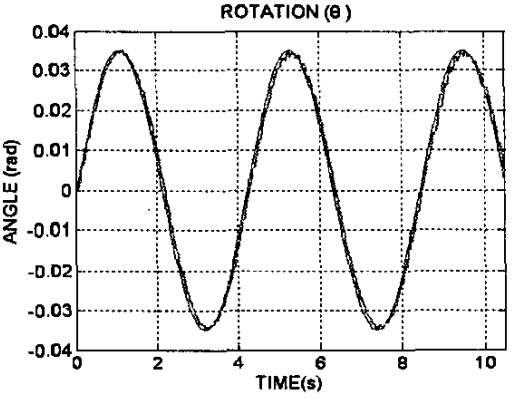

Figure 10. Rotation experiment around Z-axis.